JVI Journals.ASM.org

The Amphipathic Helix of Influenza A Virus M2 Protein Is Required for Filamentous Bud Formation and Scission of Filamentous and Spherical Particles

Kari L. Roberts,[a,b] George P. Leser,[a,b] Chunlong Ma,[a] Robert A. Lamb[a,b]

Department of Molecular Biosciences[a] and Howard Hughes Medical Institute,[b] Northwestern University, Evanston, Illinois, USA

Influenza virus assembles and buds at the infected-cell plasma membrane. This involves extrusion of the plasma membrane followed by scission of the bud, resulting in severing the nascent virion from its former host. The influenza virus M2 ion channel protein contains in its cytoplasmic tail a membrane-proximal amphipathic helix that facilitates the scission process and is also required for filamentous particle formation. Mutation of five conserved hydrophobic residues to alanines within the amphipathic helix (M2 five-point mutant, or 5PM) reduced scission and also filament formation, whereas single mutations had no apparent phenotype. Here, we show that any two of these five residues mutated together to alanines result in virus debilitated for growth and filament formation in a manner similar to 5PM. Growth kinetics of the M2 mutants are approximately 2 logs lower than the wild-type level, and plaque diameter was significantly reduced. When the 5PM and a representative double mutant (I51A-Y52A) were introduced into A/WSN/33 M2, a strain that produces spherical particles, similar debilitation in viral growth occurred. Electron microscopy showed that with the 5PM and the I51A-Y52A A/Udorn/72 and WSN viruses, scission failed, and emerging virus particles exhibited a "beads-on-a-string" morphology. The major spike glycoprotein hemagglutinin is localized within lipid rafts in virus-infected cells, whereas M2 is associated at the periphery of rafts. Mutant M2s were more widely dispersed, and their abundance at the raft periphery was reduced, suggesting that the M2 amphipathic helix is required for proper localization in the host membrane and that this has implications for budding and scission.

Influenza A virus, a member of the *Orthomyxoviridae*, is an enveloped virus with a negative-strand segmented RNA genome. In virions, the eight RNA segments are decorated with the nucleocapsid protein (NP) and an RNA-dependent RNA polymerase (Pol) complex. The ribonucleoproteins (RNPs) are enclosed within a lipid bilayer supported by an internal coat of matrix protein (M1). The viral integral membrane proteins hemagglutinin (HA), neuraminidase (NA), and the M2 ion channel protein are anchored in the viral envelope. During infection the viral RNA is replicated in the nucleus, and it subsequently associates with the viral nucleoprotein (NP) and the RNA polymerase subunits (PA, PB1, and PB2). Assembled RNPs exit the nucleus through nuclear pores and traffic along microtubules to the plasma membrane (1). M1 interacts with the viral RNP at neutral pH (2–4) and together with HA, NA, and M2 assembles into viral particles at the plasma membrane. In polarized cells, budding takes place on the apical surface preferentially at highly organized patches of lipids termed lipid rafts (5, 6). Viral envelopes derived from lipid rafts are highly enriched in cholesterol and contain large amounts of glycerophospholipids and sphingolipids (7).

In the virus-infected cell, HA associates with lipid rafts (8, 9), which coalesce to form "barges" of rafts (from ~325 to 500 nm at 4 h postinfection [p.i.] to ~425 to 600 nm at 6 h p.i.), with HA colocalizing with the ganglioside lipid raft marker GM1 (9). M2 protein associates mainly with the periphery of lipid rafts and is largely excluded from virions. In contrast, M1 cannot target the plasma membrane in the absence of other viral proteins (10, 11). M1 expressed alone in cells cannot form virus-like particles (12) and likely targets the plasma membrane by associating with the cytoplasmic tails of the viral transmembrane proteins such as HA, NA (13, 14), and M2 (11, 15).

Many strains of influenza virus bud as spherical particles (approximately 100 nm in diameter) while others produce long filaments (up to 20 μm in length). For example, A/WSN/33 (H1N1) (herein designated WSN) buds largely as spherical virions, whereas A/Udorn/72 (H3N2) (herein designated Udorn) produces a mixed population of spherical and filamentous virions in MDCK cells. It is unclear if spherical or filamentous viruses have advantages over one another as both appear to be similarly infectious (16) and contain a single copy of the viral genome (17–20). It is noteworthy that spherical and filamentous viruses have separate primary entry pathways (21, 22). The dominant morphology of viruses isolated from the upper respiratory tract of human patients is filamentous (19, 20), suggesting that filamentous influenza virus is more relevant clinically and may have a selective advantage in circulating strains. It is well established that serial passage of a filamentous strain in embryonated chicken eggs results in selection of spherical particles (23). Thus, dominance of spherical virus production in cell culture may be caused by a loss in environmental selectors. Previous studies have shown that filamentous virus production is dependent upon M1 (16, 24–26) as well as Rab11 and Rab11-interacting proteins (27). In addition it has been shown that conserved residues within an amphipathic helix in the membrane-proximal region of the M2 cytoplasmic tail

Received 21 May 2013 **Accepted** 30 June 2013
Published ahead of print 10 July 2013
Address correspondence to Robert A. Lamb, ralamb@northwestern.edu.

doi:10.1128/JVI.01363-13

are required for viral filament formation (28) as well as facilitating fission of budding membrane *in vitro* (29).

The M2 protein is a homotetramer of 97 amino acids per monomer consisting of a small N-terminal ectodomain (24 residues), a transmembrane domain (residues 25 to 43), and a long cytoplasmic tail (residues 44 to 97) (30). M2 is a multifunctional protein and has a pH-activated ion channel activity that selectively gates protons into the viral interior during uncoating when the virion has been endocytosed and is in the acidic environment of the endosomal lumen. Acidification of the virion causes dissociation of M1 protein from the viral RNP, a prerequisite for transport of the RNPs into the nucleus (31). M2 is also involved in virion budding and scission during viral assembly. M2 residues 45 to 62 form an amphipathic helix (32–34) and make up a critical region for filamentous budding and efficient scission. In many influenza virus strains, M2 contains up to four possible cholesterol recognition/interaction amino acid consensus (CRAC) motifs that overlap the helix domain; however, Udorn virus is a rare example of a strain that does not contain a CRAC motif that fits the L/V-X_{1-5}-Y-X_{1-5}-R/K consensus sequence. A cysteine residue at position 50 is covalently modified with palmitate and could play an role in anchoring M2 to the membrane though this modification has been shown to have only minor effects on virulence in mice (35) and membrane targeting in mammalian cells (36, 37).

Previous reports from our laboratory have demonstrated that five highly conserved residues within the hydrophobic face of the M2 amphipathic helix (shown in red text in Fig. 1A and B) are required for viral filament formation in cells infected with the Udorn strain. A mutant virus containing alanine substitutions for all five of these conserved residues (M2 five-point mutant, or 5PM) forms almost entirely spherical virions, whereas single alanine mutations within the set of five bulky residues are insufficient to alter virion morphology (28). These studies additionally demonstrated that these five hydrophobic residues within the M2 amphipathic helix are required for proper scission of the emerging viral envelope. Virus with single alanine mutations within this set of five residues exhibited a normal M2 phenotype (28). To determine the minimum region of the amphipathic helix required for scission, the five conserved hydrophobic residues were mutated two at a time, and their effect on virus growth and morphology was examined. The data show that any two of these hydrophobic residues mutated together to alanines in the Udorn virus strain result in a loss of filamentous virus formation, reduced viral fitness, and scission.

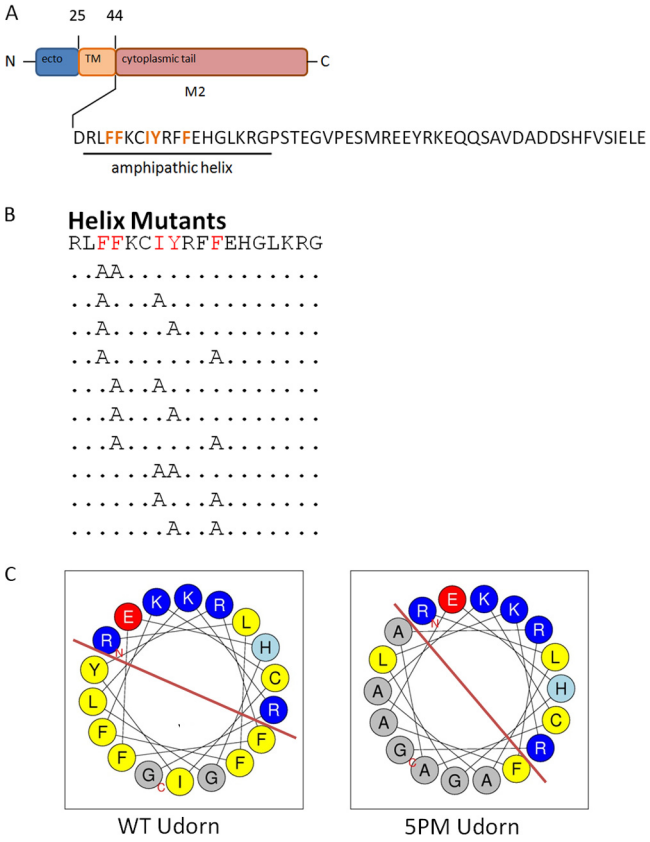

FIG 1 M2 amphipathic helix mutants. (A) Map of M2 structure depicting the ectodomain (ecto), transmembrane domain (TM), and cytoplasmic tail. The amphipathic helix located between the transmembrane domain and cytoplasmic tail is underlined. Amino acid sequence is of the A/Udorn/72 strain. (B) Sequence of M2 amphipathic helix, with residues mutated to alanines in the 5PM virus shown in red. The residues in red were mutated two at a time to alanines. Amino acid sequence is that of the A/Udorn/72 strain. (C) Helical wheel plots illustrating the basic and polar faces of the M2 amphipathic helix separated by a red line. The image was created using HeliQuest software (http://heliquest.ipmc.cnrs.fr/).

MATERIALS AND METHODS

Cells and reagents. Madin-Darby canine kidney (MDCK) and 293T cells were maintained in Dulbecco's modified Eagle's medium (DMEM) supplemented with 10% fetal bovine serum (FBS). MDCK cells stably expressing wild-type (wt) Udorn M2 protein (M2-MDCK) were maintained in DMEM with 10% FBS, 200 μg/ml Geneticin (G418; InvivoGen, San Diego, CA), and 2 μM amantadine (Sigma-Aldrich, St. Louis, MO). All cells were maintained in a humidified incubator containing 5% CO_2 at 37°C.

Mutant virus construction. Recombinant Udorn and WSN viruses were constructed by reverse genetics, as described previously (15, 38). Briefly, eight plasmids with the eight influenza virus RNA segments under the control of a Pol I promoter and four plasmids encoding PB1, PB2, PA, and NP under the control of a Pol II promoter were used to transfect subconfluent 293T cells in six-well dishes. At 15 h posttransfection, the medium was replaced with 2 ml of OptiMEM containing 3 μg/ml *N*-acetyl trypsin (NAT; Sigma-Aldrich). Six hours after the medium was changed, the cells had detached from the dish, and clumps were disrupted by up and down pipetting. The cells and medium were transferred to subconfluent MDCK cells grown in six-well dishes. After 48 to 60 h, the supernatant was collected and clarified by centrifugation, and virus titers were determined by plaque assay (described below) on M2-MDCK cells. The Udorn virus M2 five-point mutant (5PM) was constructed previously (28). To create the additional M2 mutants, the M segment pHH21 plasmid was mutated using QuikChange mutagenesis (Stratagene, La Jolla, CA). To ensure that the mutant viruses contained the expected mutation, viral RNA was extracted using a QIAamp viral RNA kit (Qiagen, Valencia, CA) and transcribed to DNA using Super Reverse Transcriptase (Molecular Genetic Resources, Tampa, FL) and amplified with AmpliTaq DNA polymerase (Applied Biosystems, Foster City, CA). The nucleotide sequence of the complete RNA segment 7 M gene was determined by using a 3100-Avant genetic analyzer (Applied Biosystems).

Immunofluorescence microscopy. MDCK cells were grown on glass coverslips and infected with wt Udorn virus or viruses containing the M2 mutations at a multiplicity of infection (MOI) of 3. Infection was synchronized by allowing viral attachment at 4°C for 1 h, followed by a wash in phosphate-buffered saline (PBS) and overlay of warmed (37°C) DMEM–1% penicillin and streptomycin supplemented with 1 μg/ml NAT. Infected cells were fixed with 10% formalin (Electron Microscopy

Sciences, Hatsfield, PA) at 8.5 h postinfection (p.i.). Cell surfaces were blocked with 10% normal donkey serum (Sigma-Aldrich) in PBS, followed by immunostaining (without permeabilization) with goat anti-H3 HA antibody (derived from influenza A/Aichi/2/68 virus; National Institute of Allergy and Infectious Disease Repository, Bethesda, MD) at a concentration of 1:400 in PBS–1% bovine serum albumin (BSA). Bound primary antibody was labeled with Alexa Fluor 488-conjugated anti-goat IgG (Invitrogen, Eugene, OR) at a concentration of 1:200 in PBS–1% BSA. Coverslips were mounted onto glass slides using Prolong Gold (Invitrogen) and left to set overnight in the dark. Immunostained cells were imaged with an LSM 5 Zeiss (Thornwood, NY) confocal microscope using a 63× objective. Collected images were modified using Adobe Photoshop CS3.

Thin-section transmission electron microscopy. To visualize budding complexes on cell surfaces, MDCK cells were mock infected or infected with the wt, the 5PM, or the I51A-Y52A mutant Udorn or WSN virus at an MOI of 3 as described above. At 12 h p.i. (Udorn) or 6 h p.i. (WSN), cells were transferred to 4°C and subsequently stained with antibodies, embedded in resin, and processed for transmission electron microscopy as previously described (9). The antibodies used were specific for M2 (monoclonal antibody 14C2) (39), for Udorn HA (goat antiserum specific for A/Equine/Miami/1/63 HA [3]), or for WSN HA (chicken antiserum against A/Puerto Rico/8/34 HA [1]). Antibody binding was visualized by using host-specific secondary antibodies raised in donkeys and conjugated with either 6-nm (M2) or 12-nm (HA) gold particles (Jackson ImmunoResearch Laboratories, Inc., West Grove, PA). Thin sections were contrasted by staining with uranyl acetate and lead citrate. Samples were examined in a JEOL 1230 electron microscope operating at 80 kV and imaged with a Gatan 831 charge-coupled-device (CCD) camera.

Coassociation of HA and M2 in planar sheets of plasma membrane. MDCK cells were infected with Udorn at an MOI of 3. At 12 h p.i., the cells were placed at 4°C and blocked with 0.2% ovalbumin and 0.1% normal donkey serum in 100 mM NaCl, 5 mM KCl, 1 mM $CaCl_2$, 1 mM $MgSO_4$, and 1 mM NaH_2PO_4, pH 7.4. Cells were stained with antibodies specific for Udorn HA and M2, followed by host-specific secondary immunoglobulin conjugated to 12-nm (HA) or 6-nm (M2) gold particles. In all cases, antibodies were diluted in blocking buffer with 0.1% BSA-c (Electron Microscopy Sciences, Hatfield, PA). Preparation of membrane sheets was done as described originally by Sanan and Anderson (40) and was carried out essentially as described previously (15). Images of samples were taken at a magnification of 40,000 and encompassed approximately 11.1 μm^2 of plasma membrane. At least 10 images were analyzed for each experimental condition, with each image representing a different cell plasma membrane.

The location of gold particles was marked manually using Adobe Photoshop CS3 (Adobe Systems Inc., San Jose, CA). The resulting images were segmented and an *x*/*y* coordinate list for all the gold markers in an image was generated using ImageJ (http://rsb.info.nih.gov/ij/). The Ripley analysis (41), which examines the expected number of neighbors within a specified distance given the number of points in the sampled area and compares these to a sample random distribution, was done using the SpatStat library (42) for the statistical analysis of spatial data in R (http://www.R-project.org). Simulations of 100 populations of random points were used to generate envelopes describing complete spatial randomness.

Plaque assays of influenza Udorn and WSN viruses. To determine viral titers and plaque diameter, confluent MDCK or M2-MDCK cells grown in 60-mm dishes were infected with virus suspended in 500 μl of DMEM–1% BSA and incubated with agitation at 4°C for 1 h. Virus inoculum was removed, and cells were washed in PBS and overlaid with a 1:1 mixture of 2.4% Avicel (FMC, Newark, DE) and 2× DMEM–10 mM HEPES–2% penicillin and streptomycin plus 1 μg/ml L-1-tosylamide-2-phenylmethyl chloromethyl ketone (TPCK)-treated trypsin (Worthington, Lakewood, NJ). At 48 h p.i., the overlay was removed, and cells were stained with blue-black stain (1 g naphthalene black, 110 ml glacial acetic acid, 13.6 g of sodium acetate, anhydrous, and H_2O to 1 liter) for 30 min.

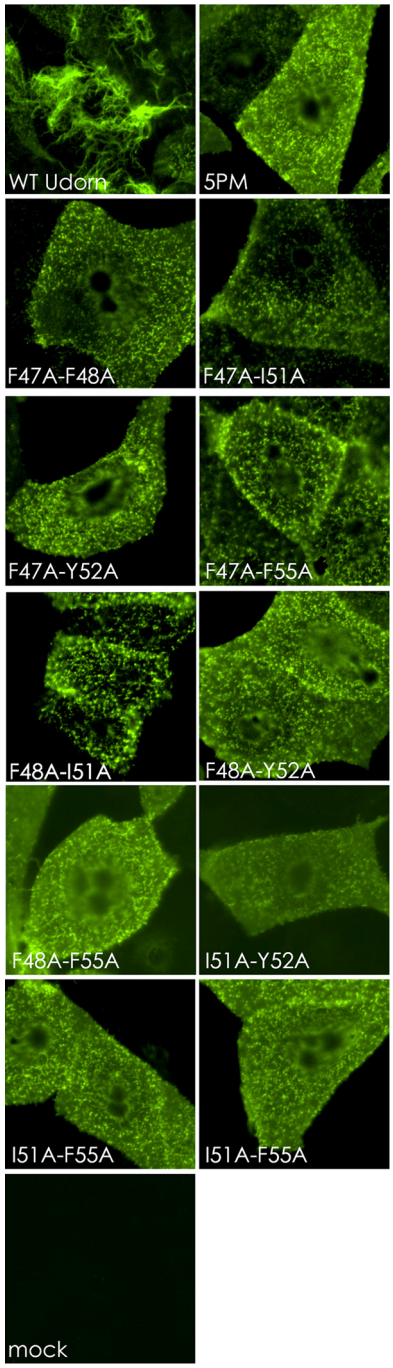

FIG 2 M2 helix mutants do not produce filamentous virus. Images are of MDCK cells infected with wt or mutant Udorn virus at an MOI of 3. Cells were fixed at 8.5 h p.i. and stained with antibody to HA (green).

After incubation, the stain was removed, and cells were gently washed with water and left to dry. Plaque diameters were measured using ImageJ.

Two-electrode voltage clamp analysis of *Xenopus* oocytes expressing wt and mutant M2 proteins. To construct the 10 unique alanine substitution mutants in the M2 amphipathic helix mutants in a suitable vector for expression of mRNA in oocytes of *Xenopus laevis*, the wt M2 open reading frame was cloned into the pSUPER vector; M2 was subjected to mutagenesis by using QuikChange mutagenesis, and the sequence was verified. Detailed methods of oocyte preparation and maintenance and of

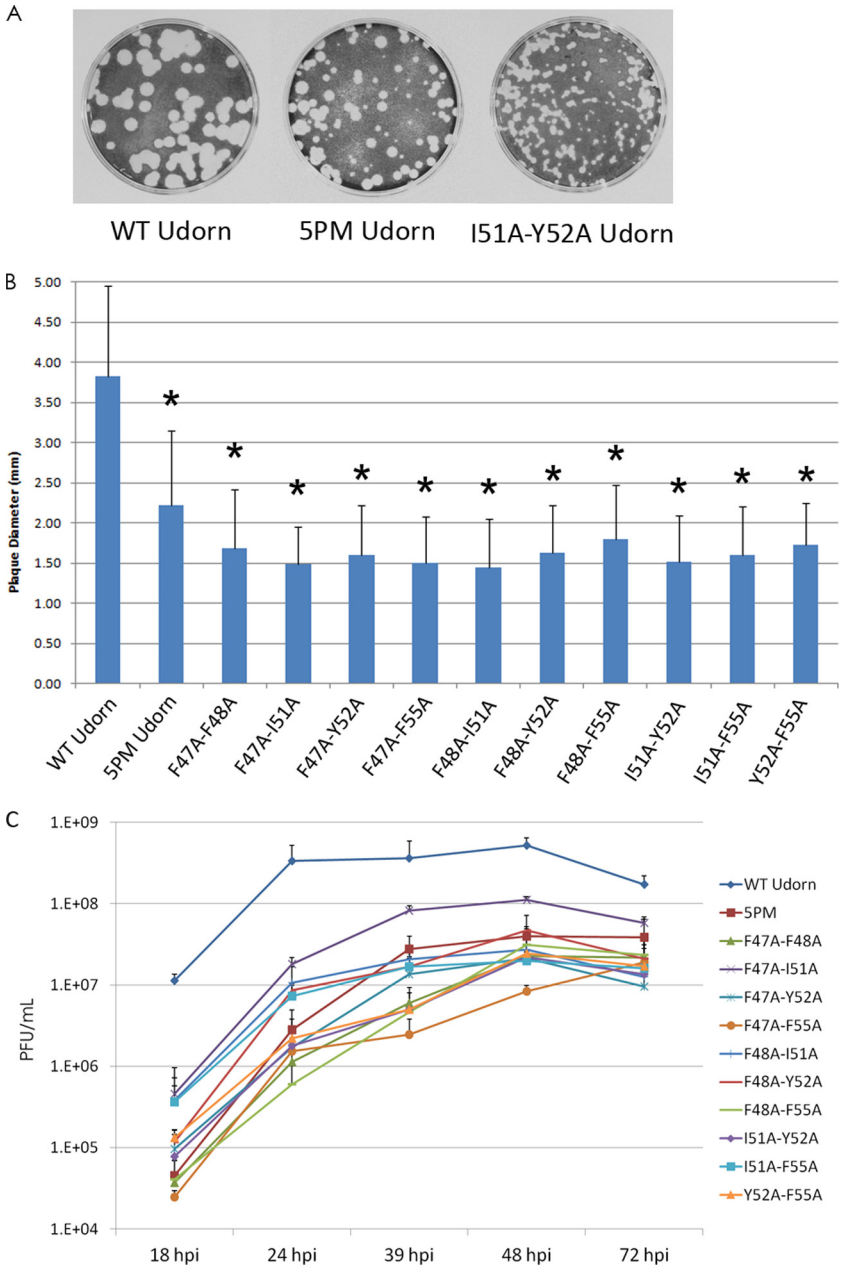

FIG 3 M2 (Udorn) helix mutants produce smaller plaques than the wt virus and have reduced growth kinetics. (A and B) The plaque assay of Udorn virus was performed using MDCK cells infected with wt or mutant influenza virus. Cells were overlaid with Avicel-DMEM following a 1-h incubation at 4°C to allow viral detachment. After 48 h of incubation at 37°C, cells were stained to reveal plaques. Plaque diameters were measured using ImageJ, and a *t* test was performed to measure differences between diameters. Asterisks indicate a statistical difference in diameter compared to the wt ($P < 0.05$). (C) MDCK cells were infected with wt or mutant virus at an MOI of 0.001. The supernatant was collected at the shown times p.i., and the titer was determined by plaque assay. All data points were done in triplicate. hpi, hours postinfection.

mRNA synthesis and microinjection were described previously (43). In this study, 50 ng of mRNA was injected into each oocyte. At 48 h after injection, whole-cell surface currents were measured by using a two-electrode voltage clamp apparatus. Currents were acquired and analyzed using pClamp, version 10.0, software (Axon Instruments).

RESULTS

Double mutation of the amphipathic helix of M2 ablates budding of filamentous virions and restricts virus growth. To determine the minimum region of the amphipathic helix necessary for filamentous budding and for efficient scission, reverse genetics (15, 38) was used to make mutations in the amphipathic helix. Two hydrophobic residues were changed simultaneously such that all possible combinations of pairs of the five hydrophobic residues mutated in the 5PM M2 protein were mutated to alanine (Fig. 1B). To ensure that there were no unanticipated mutations, the entire RNA segment 7 encoding the M1 and M2 proteins for each mutant virus was sequence verified (data not shown). A helical wheel plot (Fig. 1C) illustrates the location of these alanine

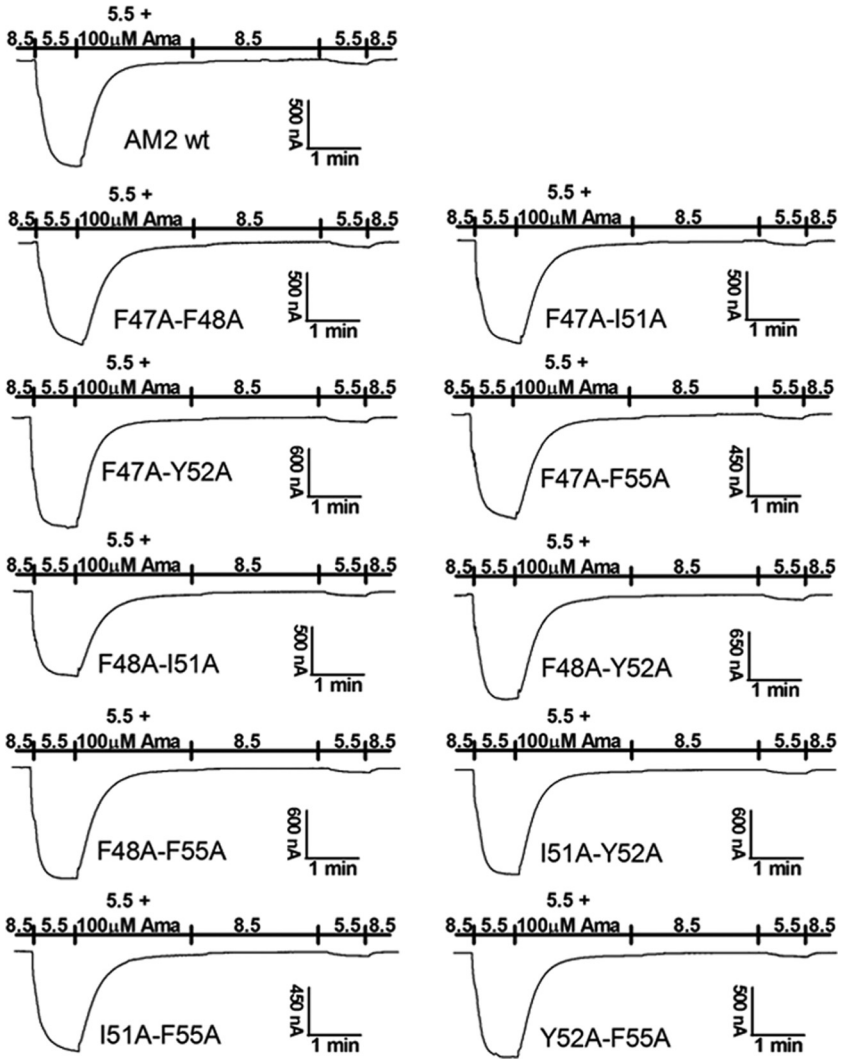

FIG 4 pH-activated proton current and amantadine sensitivity of wt M2 and mutant ion channels. wt Udorn M2 and mutant M2 ion channels were expressed in oocytes of *Xenopus laevis*, and surface currents were measured using a two-electrode voltage clamp apparatus. Ion channels were activated by using a bathing solution of pH 5.5. Representative recordings of these ion channels are shown. Amantadine sensitivity was evaluated by bathing oocytes in pH 5.5 solution containing 100 μM amantadine when the surface current reached maximum.

substitutions for the 5PM compared to wild-type (wt) Udorn M2 protein. Basic residues are shown in blue, acidic are in red, hydrophobic are in yellow, and alanine and glycine are in gray. A red line separates the polar and hydrophobic faces of the helix.

Immunostaining and confocal fluorescence microscopy were used to visualize the phenotype of budding virus from wt Udorn and M2 mutant virus-infected MDCK cells using antibody specific for hemagglutinin (HA). It was observed that MDCK cells infected with the wt virus contain long filamentous virions extending from the cell surface as well as a lesser amount of spherical budding (Fig. 2). The M2 double mutants exhibited a very different morphology from wt virus in that very few viral filaments were observed budding from the cell surface, and the vast majority of these virus particles budded as small spheroid-like buds. M2 double mutant viruses that emerged from the surface of MDCK cells were indistinguishable in morphology from budding particles from cells infected with 5PM virus (Fig. 2).

To address whether the mutant M2 viruses were attenuated for growth, a plaque assay was performed in MDCK cells, and the plaque sizes of the mutant viruses were compared to the plaque size of wt virus. As shown in Fig. 3A and B, wt Udorn virus formed large (4-mm) plaques, whereas the 5PM and all the M2 double mutants had a reduced diameter (Fig. 3A and B). A *t* test verified that the mutant M2 virus plaque sizes were statistically different from wt plaques (P of >0.05) and that there was no statistical difference between mutant M2 plaque sizes.

In addition to differences in average plaque diameters, it was noted that all viruses produced a mixed population of large and small plaques within a single dish of infected cells. One interpretation of this difference in plaque sizes is that genetically distinct populations of virus were present within the virus stock. To test this notion, large and small plaques were picked from the wt and 5PM and from a representative M2 double mutant (I51A-Y52A) virus and replaqued. In every case, virus from individual picked plaques formed both large and small plaques in the assay (data not shown), indicating that the trait bred true.

The growth kinetics of wt and mutant M2 viruses were determined by performing a multistep growth curve. The data indicate that all M2 mutants were debilitated in growth at every tested time point compared to wt virus (Fig. 3C). Despite the more extensive mutations in the 5PM M2, its growth curve fell within the middle of the M2 double mutants. This 1- to 2-log decrease in titer for the 5PM is less severe than the 5-log decrease from a previous report with this recombinant Udorn M2 mutant (28); the result was also more comparable to the reported growth kinetics in a transcomplementation assay though we did not observe recovery to wt titers at 48 h p.i. as was reported using this different assay (44). The growth curves of the mutant viruses correlate with the sizes of the plaques formed by the mutant viruses.

The M2 amphipathic helix mutations do not affect M2 ion channel activity. To determine if the M2 amphipathic helix double mutants affected the M2 proton-selective ion channel activity, which in turn could affect virus growth, the ion channel activities of the mutant M2 proteins were measured using oocytes of *Xenopus laevis* expressing M2 and a two-electrode voltage clamp procedure. The M2-specific current was measured after bathing oocytes in pH 5.5 buffer to activate the channel. Subsequent addition of the M2 ion channel blocker amantadine (100 μM for 2 min) demonstrated sensitivity since proton movement ceased after drug treatment (Fig. 4). All double M2 mutants demonstrated ion channel activity similar to that of the wt, including sensitivity to amantadine (Fig. 4). The ion channel activity of the 5PM M2 had been shown previously to be indistinguishable from that of the wt M2 (28). The data suggest that the growth defects cannot be a result of a defect in ion channel activity.

M2 double mutants in the influenza WSN virus genetic background. In tissue culture, the Udorn strain buds predominantly as long filaments, whereas the WSN strain buds nearly exclusively as spherical particles. The Udorn M2 mutant growth defect is concomitant with a loss in filamentous morphology, which raises the possibility that the M2 mutations may be relevant only to filamentous strains. To test this hypothesis, the 5PM M2 and the M2 I51A-Y52A, as a representative of the double M2 mutants, were introduced into the influenza WSN virus genetic background by reverse genetics. The plaque sizes and growth kinetics of the wt WSN and WSN M2 mutant viruses are shown in Fig. 5A and B.

wt WSN virus forms plaques with an average diameter of 2 mm after 48 h p.i. The WSN 5PM and I51A-Y52A M2 mutant viruses made plaques approximately 1 and 1.5 mm in diameter, respectively, at 48 h p.i. Both the WSN 5PM and I51A-Y52A M2 mutant viruses had plaque diameters that were statistically different from the diameter of wt WSN virus plaques, as indicated by a *t* test ($P > 0.05$). The smaller plaque size observed with the WSN 5PM is approximately the same percent decrease (50%) in diameter observed with the Udorn 5PM compared to their respective wt virus plaque sizes (Fig. 3).

In parallel to the reduced plaque diameter, WSN M2 mutants were attenuated for viral growth kinetics in a multistep growth curve. MDCK cells were infected at an MOI of 0.001 with wt WSN, WSN 5PM, or WSN M2 I51A-Y52A, and virus titers were determined at the times indicated in Fig. 5C. The WSN 5PM grew approximately 1 to 2 logs more slowly than the wt WSN virus at all time points. The WSN M2 I51A-Y52A mutant virus was less attenuated, reaching wt titers by 48 h p.i., but was debilitated in growth to a similar extent as the WSN 5PM virus at earlier time points (1 to 2 logs lower than the wt from 18 to 39 h p.i.). Thus,

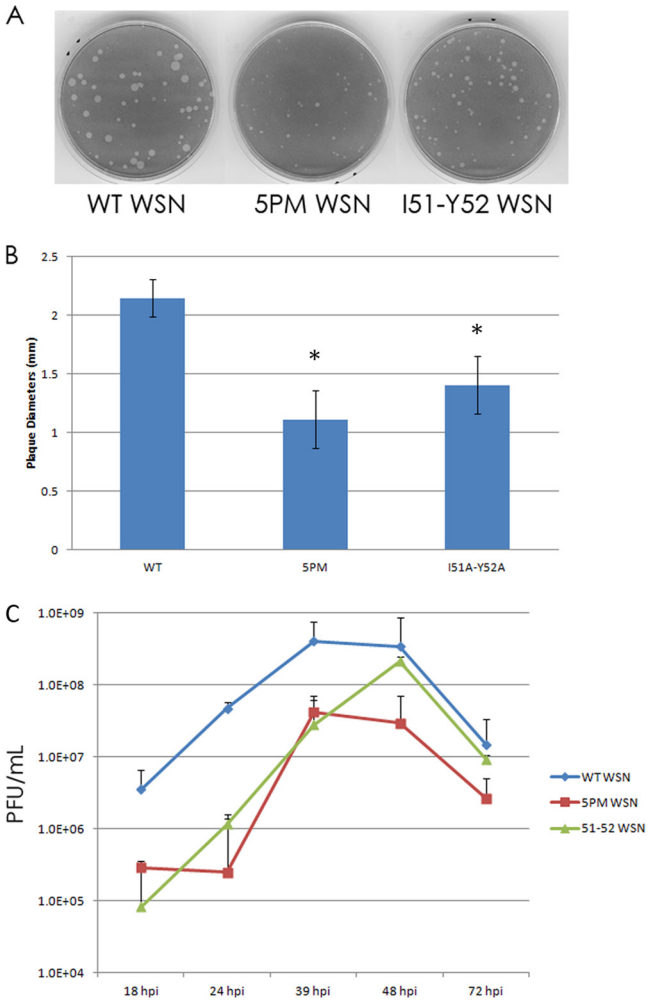

FIG 5 M2 (WSN) amphipathic helix mutants produce smaller plaques than the wt virus and have reduced growth kinetics. (A and B) The plaque assay was performed using MDCK cells infected with wt WSN or M2 mutant influenza virus. Cells were overlaid with Avicel-DMEM following a 1-h incubation at 4°C to allow viral detachment. After 48 h of incubation at 37°C, cells were stained to reveal plaques. Plaque diameters were measured using ImageJ, and a *t* test was performed to measure differences between diameters. Asterisks indicate a statistical difference in diameter compared to the wt ($P < 0.05$). (C) MDCK cells were infected with wt or mutant WSN virus at an MOI of 0.001. The supernatant was collected at the listed times, and the titer was determined by plaque assay. All data points were done in triplicate.

whereas the M2 I51A-Y52A mutation in the WSN background is somewhat less attenuated than the 5PM virus, both viruses have considerable growth defects compared to wt WSN virus.

Both Udorn M2 virus mutants and WSN M2 virus mutants exhibit incomplete scission. To examine the morphology of budding virions, MDCK cells were infected with wt Udorn or wt WSN virus or with the WSN mutant 5PM or M2 I51A-Y52A (as a representative double mutant) virus, and at 12 h p.i. (Udorn) or 6 h p.i. (WSN) the cells were prepared for thin sectioning and immunostaining using gold-conjugated antibody to HA and M2 (12-nm and 6-nm gold particles, respectively). Representative images are shown in Fig. 6A to D (Udorn) and 7 A to D (WSN).

Thin sections of the cells infected with wt Udorn virus exhibited long filamentous particles budding from cells, with the viral

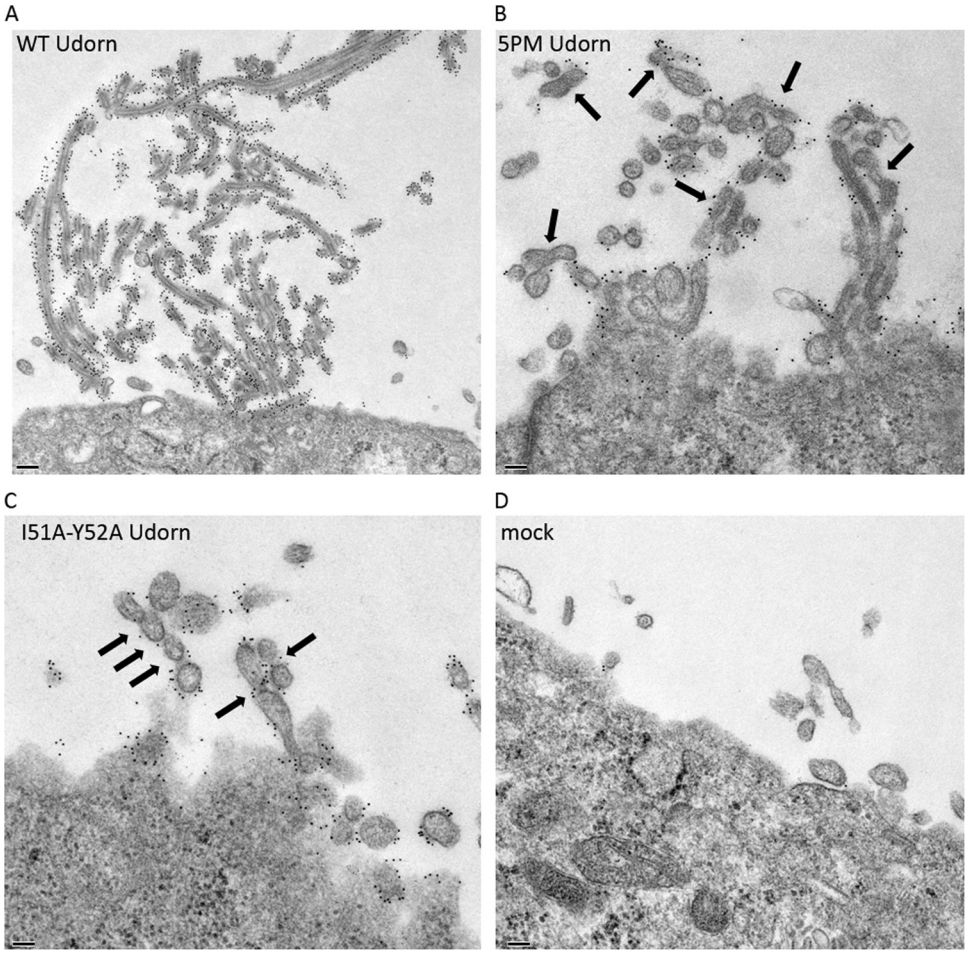

FIG 6 Udorn M2 mutants exhibit incomplete scission. Thin sections from Udorn-infected MDCK cells at 12 h p.i. immunostained with gold-conjugated antibody indicate HA (12 nm) and M2 (6 nm) localization. Arrows indicate an apparent joined membrane between two virus particles. Scale bars, 0.2 μm (A) and 0.1 μm (B to D).

envelopes separated distinctly from other virions (Fig. 6A). In contrast, the Udorn 5PM and I51A-Y52A M2 mutants exhibited a bulbous morphology and were much shorter and more pleomorphic than wt Udorn virions (Fig. 6B and C). The Udorn M2 mutant virus particles exhibited several examples of failed scission attempts ("beads on a string") (examples are indicated with black arrows in Fig. 6B and C).

Both wt and M2 mutant WSN viruses budded as spherical particles from infected host cell membranes (Fig. 7A to C). However, in contrast to wt WSN virions, the WSN 5PM and I51A-Y52A M2 mutants exhibited many examples of incomplete scission (Fig. 7B and C, black arrows) and formed clump-like layers of virus that could be seen along large sections of the plasma membrane. wt WSN tended to bud as individual particles, and single layers of budding virus were the dominant phenotype (Fig. 7A). Thus, while mutations within the WSN M2 amphipathic helix do not result in alterations to virion morphology, the mutations do affect scission of spherical virions. These data reinforce previously reported scission defects with the Udorn 5PM virus (29) and support the hypothesis that the amphipathic helix is essential for proper scission of budding influenza virus virions.

wt Udorn M2, but not mutant M2, exhibits strong coclustering with HA in infected cell membranes. It has been shown previously from analysis of HA and M2 distribution in planar membrane sheets that HA and M2 cocluster at the plasma membrane (15). The clustering was measured after immunogold staining with gold-conjugated antibody specific for HA and M2 and quantification of the distribution of HA and M2. The spatial relationship was measured using the Ripley bivariate *K* function (41, 45), a statistical method to determine the probability that a given object exists near another population of objects by chance. Details of this technique have been described previously (15, 40, 46). The Ripley analysis was used to examine one population of gold particle density in relation to a single gold particle and to represent this association as a function of distance. For example, a completely random distribution of two proteins in the linear representation of the Ripley *K* function [$L(r) - r$, where r is the radius] has a theoretical value of 0. In Fig. 8 dashed lines represent the 99% confidence interval; thus, linear transformations of the Ripley *K* function (solid lines) falling within this region are considered to have random distribution. To determine whether or not HA similarly coclusters with mutant M2 in Udorn-infected cell membranes, planar sheets from virus-infected MDCK cells were im-

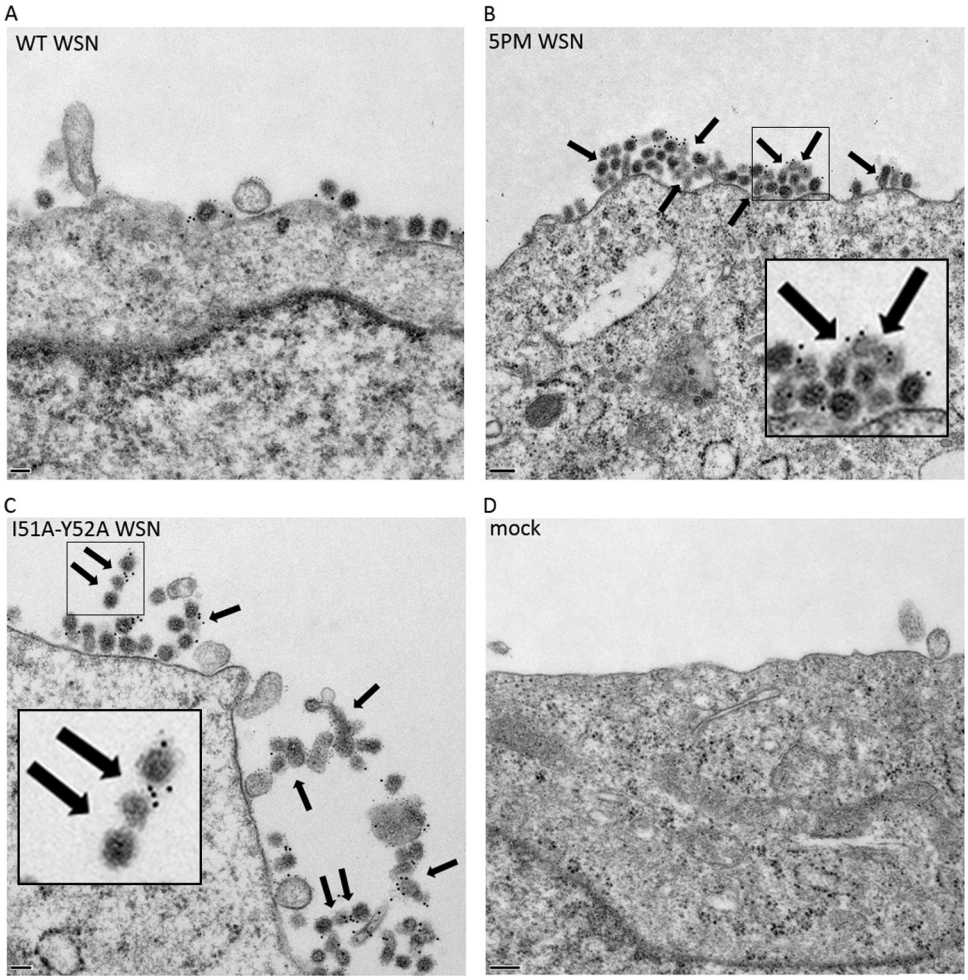

FIG 7 WSN M2 mutants exhibit incomplete scission. Thin sections from WSN-infected MDCK cells at 6 h p.i. immunostained with gold-conjugated antibody indicate HA (12 nm) and M2 (6 nm) localization. Arrows indicate an apparent joined membrane between two virus particles. Scale bars, 0.1 μm (A and C) and 0.2 μm (B and D).

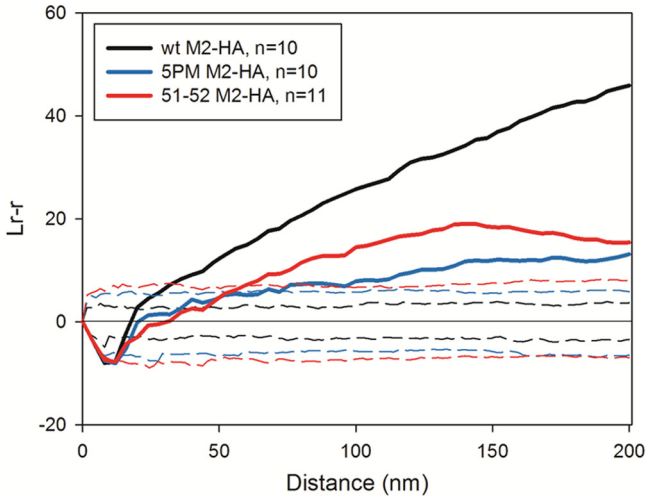

FIG 8 Statistical analysis of HA and M2 clustering. Apical membranes from MDCK cells infected with wt Udorn or M2 mutant Udorn virus were immunostained for HA and M2, and relative distributions were analyzed using the Ripley bivariate analysis. Dashed lines indicate the 99% confidence interval, and solid lines represent the Ripley *K* function. HA and M2 are considered to be coclustered at distances where the solid line is above the 99% confidence interval. 51-52, I51A-Y52A mutation.

munostained with gold particles (12- and 6-nm for HA and M2, respectively), and spatial distribution was analyzed using Ripley's bivariate *K* function. Data representing a comparison of HA and M2 clustering from at least 10 membrane sheets of different infected cells are presented in Fig. 8.

Planar membrane sheets from wt Udorn-infected cells showed that HA and M2 associate nonrandomly (Fig. 8, solid black line). This nonrandom clustering increases sharply with increased distance and supports previous observations (15). In contrast, analysis of planar membrane sheets from Udorn 5PM and M2 I51A-Y52A mutant virus-infected cells indicates markedly reduced coclustering of HA and mutant M2 though there is a very weak coclustering beginning at 75 to 100 nm. This reduced association of HA and mutant M2 is consistent with the notion that mutant M2 may not be localized in the correct domain of the host lipid bilayer and/or in the necessary density for proper budding and scission.

DISCUSSION

Segment 7 (M segment) of the influenza virus RNA genome encodes two transcripts through alternative splicing. Unspliced mRNA encodes the matrix protein M1, and spliced mRNA en-

codes M2. M1 and M2 expressed in cells coprecipitate, and amino acids 71 to 73 and 74 to 76 within M2 are required for both efficient interaction with M2 and viral filament formation (15). Several genetic studies of M1 have demonstrated a role for the matrix protein in filamentous budding (16, 24–26). Exposure of filamentous virus to the monoclonal antibody 14C2, which binds the ectodomain of M2 (39), perturbs filament formation, and escape mutants contain amino acid changes in M1 or the C-terminal tail of M2 (16, 47). Further, treatment with 5 μg/ml of 14C2 IgG restricts growth (as measured by plaque size) of the filamentous Udorn strain but does not inhibit growth of the spherical WSN influenza virus strain (39). Additional evidence to support the involvement of M2 with filamentous budding was demonstrated by experiments with Udorn virus expressing M2 truncated at amino acid 70, which results in loss of filament formation (48). Surprisingly, when this same M2 truncation mutation is introduced into the WSN background, budding virus exhibits a filamentous rather than spherical morphology (48, 49). The latter phenotype, however, is believed to be the result of delayed scission rather than true filamentous budding (48).

Amphipathic helices have long been recognized as generators and sensors of membrane curvature (50–52). Residues on the hydrophobic face of the helix insert into the membrane and anchor the helix in place while polar residues are involved in electrostatic interactions with the membrane and potentially curvature induction. While full-length M2 is a transmembrane protein and is therefore always associated with membranes, the 17-amino-acid sequence of the wt M2 amphipathic sequence is sufficient to associate with giant unilamellar vesicles (GUVs) and drive budding *in vitro* (29).

Phase-separated GUVs containing sphingomyelin, polyunsaturated phosphocholine, and cholesterol segregate into lipid-ordered (L_O) and lipid-disordered (L_D) phases that are analogous to the lipid raft (L_O) and nonraft (L_D) regions of apical membrane in cells. A fluorescently labeled peptide corresponding to the M2 amphipathic helix peptide associates with the L_D face of phase-separated GUVs and clusters at the phase boundary where the peptide drives budding of the L_O phase. Additionally, the M2 cytoplasmic tail of A/Duck/Ukrane/1/63 (H3N8) fused at its N terminus to yellow fluorescent protein was able to associate with membrane when expressed in mammalian cells though this was dependent upon an intact CRAC motif and, to a lesser extent, acylation (36). Therefore, it is tempting to speculate that the amphipathic helix of full-length M2 in virus-infected cells drives its localization to the boundary of lipid rafts, where it influences budding and scission of nascent virions.

Other recent *in silico* data support the ability of M2 to cause membrane curvature as well as demonstrate its sensitivity to penta-alanine mutations within the amphipathic helix (53). It was found that the M2 amphipathic helix is sufficient to cause negative Gaussian curvature (NGC), which is a prerequisite alteration of membrane shape for budding and scission mechanisms, similar to that proposed for influenza virus virions (28). Based on these data, M2 is capable of generating NGCs that create a neck diameter 10 times smaller than the diameter of an emerging influenza virus particle. Additionally, M2 protein-containing membrane-interacting domains and a cytoplasmic domain cooperatively promote an enhanced ability to generate NGC.

The peripheral localization of M2 near lipid rafts has been documented previously (9), and disruption of the amphipathic nature of the M2 helix may interfere with the innate ability of the helix to recognize and associate with boundaries of L_O domains, resulting in mislocalization and reduced efficacy of budding and scission. This is supported by the electron microscopy images of mutant virus particles that undergo incomplete scission (Fig. 6 and 7) and also by the membrane distribution (Ripley analysis) indicating that the M2 mutant had only a weak association with HA, a lipid raft resident protein (Fig. 8).

The data presented here demonstrate that the amphipathic helix within the M2 protein cytoplasmic tail is necessary for filamentous virus production and normal viral growth. Mutation of as few as two conserved hydrophobic residues (to alanines) resulted in a loss of filamentous budding for Udorn virions. Both WSN and Udorn strains containing the 5PM or a double mutation in the M2 amphipathic helix are attenuated for growth and scission. Because these defects were seen in both filamentous and spherical strains, the M2 amphipathic helix is thought to play an important role in budding for all influenza A virus strains.

ACKNOWLEDGMENTS

We thank members of the Lamb laboratory for valuable discussions and insight. Transmission electron microscopy was performed in Northwestern University's Biological Imaging Facility.

This research was supported by grant R01 AI-20201 (R.A.L.) from the National Institutes of Allergy and Infectious Diseases. K.L.R. is an associate, G.P.L. is a specialist, and R.A.L. is an investigator of the Howard Hughes Medical Institute. C.M. is a postdoctoral associate at Northwestern University.

REFERENCES

1. **Amorim MJ, Bruce EA, Read EKC, Foeglein Á, Mahen R, Stuart AD, Digard P.** 2011. A Rab11- and microtubule-dependent mechanism for cytoplasmic transport of influenza A virus viral RNA. J. Virol. **85:**4143–4156.
2. **Ye Z, Liu T, Offringa DP, McInnis J, Levandowski RA.** 1999. Association of influenza virus matrix protein with ribonucleoproteins. J. Virol. **73:**7467–7473.
3. **Fontana J, Cardone G, Heymann JB, Winkler DC, Steven AC.** 2012. Structural changes in influenza virus at low pH characterized by cryo-electron tomography. J. Virol. **86:**2919–2929.
4. **Elster C, Larsen K, Gagnon J, Ruigrok RW, Baudin F.** 1997. Influenza virus M1 protein binds to RNA through its nuclear localization signal. J. Gen. Virol. **78:**1589–1596.
5. **Nayak DP, Balogun RA, Yamada H, Zhou ZH.** 2009. Influenza virus morphogenesis and budding. Virus Res. **143:**147–161.
6. **Rossman JS, Lamb RA.** 2011. Influenza virus assembly and budding. Virology **411:**229–236.
7. **Gerl MJ, Sampaio JL, Urban S, Kalvodova L, Verbavatz J-M, Binnington B, Lindemann D, Lingwood CA, Shevchenko A, Schroeder C, Simons K.** 2012. Quantitative analysis of the lipidomes of the influenza virus envelope and MDCK cell apical membrane. J. Cell Biol. **196:**213–221.
8. **Hess ST, Kumar M, Verma A, Farrington J, Kenworthy A, Zimmerberg J.** 2005. Quantitative electron microscopy and fluorescence spectroscopy of the membrane distribution of influenza hemagglutinin. J. Cell Biol. **169:**965–976.
9. **Leser GP, Lamb RA.** 2005. Influenza virus assembly and budding in raft-derived microdomains: a quantitative analysis of the surface distribution of HA, NA and M2 proteins. Virology **342:**215–227.
10. **Thaa B, Herrmann A, Veit M.** 2009. The polybasic region is not essential for membrane binding of the matrix protein M1 of influenza virus. Virology **383:**150–155.
11. **Wang D, Harmon A, Jin J, Francis DH, Christopher-Hennings J, Nelson E, Montelaro RC, Li F.** 2010. The lack of an inherent membrane targeting signal is responsible for the failure of the matrix (M1) protein of influenza A virus to bud into virus-like particles. J. Virol. **84:**4673–4681.
12. **Chen BJ, Leser GP, Morita E, Lamb RA.** 2007. Influenza virus hemag-

glutinin and neuraminidase, but not the matrix protein, are required for assembly and budding of plasmid-derived virus-like particles. J. Virol. **81:**7111–7123.
13. **Barman S, Ali A, Hui EKW, Adhikary L, Nayak DP.** 2001. Transport of viral proteins to the apical membranes and interaction of matrix protein with glycoproteins in the assembly of influenza viruses. Virus Res. **77:**61–69.
14. **Jin H, Leser GP, Zhang J, Lamb RA.** 1997. Influenza virus hemagglutinin and neuraminidase cytoplasmic tails control particle shape. EMBO J. **16:** 1236–1247.
15. **Chen BJ, Leser GP, Jackson D, Lamb RA.** 2008. The influenza virus M2 protein cytoplasmic tail interacts with the M1 protein and influences virus assembly at the site of virus budding. J. Virol. **82:**10059–10070.
16. **Roberts PC, Lamb RA, Compans RW.** 1998. The M1 and M2 proteins of influenza A virus are important determinants in filamentous particle formation. Virology **240:**127–137.
17. **Calder LJ, Wasilewski S, Berriman JA, Rosenthal PB.** 2010. Structural organization of a filamentous influenza A virus. Proc. Natl. Acad. Sci. U. S. A. **107:**10685–10690.
18. **Noda T, Sagara H, Yen A, Takada A, Kida H, Cheng RH, Kawaoka Y.** 2006. Architecture of ribonucleoprotein complexes in influenza A virus particles. Nature **439:**490–492.
19. **Chu CM, Dawson IM, Elford WJ.** 1949. Filamentous forms associated with newly isolated influenza virus. Lancet **i:**602.
20. **Kilbourne ED, Murphy JS.** 1960. Genetic studies of influenza viruses. I. Viral morphology and growth capacity as exchangeable genetic traits. Rapid *in ovo* adaptation of early passage Asian strain isolates by combination with PR8. J. Exp. Med. **111:**387–406.
21. **de Vries E, Tscherne DM, Wienholts MJ, Cobos-Jimenez V, Scholte F, Garcia-Sastre A, Rottier PJ, de Haan CA.** 2011. Dissection of the influenza A virus endocytic routes reveals macropinocytosis as an alternative entry pathway. PLoS Pathog. **7:**e1001329. doi:10.1371/journal.ppat.1001329.
22. **Rossman JS, Leser GP, Lamb RA.** 2012. Filamentous influenza virus enters cells via macropinocytosis. J. Virol. **86:**10950–10960.
23. **Choppin PW, Murphy JS, Tamm I.** 1960. Studies of two kinds of virus particles which comprise influenza A2 virus strains. III. Morphological characteristics: independence of morphological and functional traits. J. Exp. Med. **112:**945–952.
24. **Bourmakina SV, Garcia-Sastre A.** 2003. Reverse genetics studies on the filamentous morphology of influenza A virus. J. Gen. Virol. **84:**517–527.
25. **Burleigh LM, Calder LJ, Skehel JJ, Steinhauer DA.** 2005. Influenza A viruses with mutations in the M1 helix six domain display a wide variety of morphological phenotypes. J. Virol. **79:**1262–1270.
26. **Elleman CJ, Barclay WS.** 2004. The M1 matrix protein controls the filamentous phenotype of influenza A virus. Virology **321:**144–153.
27. **Bruce EA, Digard P, Stuart AD.** 2010. The Rab11 pathway is required for influenza A virus budding and filament formation. J. Virol. **84:**5848–5859.
28. **Rossman JS, Jing X, Leser GP, Balannik V, Pinto LH, Lamb RA.** 2010. Influenza virus M2 ion channel protein is necessary for filamentous virion formation. J. Virol. **84:**5078–5088.
29. **Rossman JS, Jing X, Leser GP, Lamb RA.** 2010. Influenza virus M2 protein mediates ESCRT-independent membrane scission. Cell **142:**902–913.
30. **Lamb RA, Zebedee SL, Richardson CD.** 1985. Influenza virus M_2 protein is an integral membrane protein expressed on the infected-cell surface. Cell **40:**627–633.
31. **Pinto LH, Lamb RA.** 2007. Controlling influenza virus replication by inhibiting its proton channel. Mol. Biosyst. **3:**18–23.
32. **Nguyen PA, Soto CS, Polishchuk A, Caputo GA, Tatko CD, Ma C, Ohigashi Y, Pinto LH, DeGrado WF, Howard KP.** 2008. pH-induced conformational change of the influenza M2 protein C-terminal domain. Biochemistry **47:**9934–9936.
33. **Schnell JR, Chou JJ.** 2008. Structure and mechanism of the M2 proton channel of influenza A virus. Nature **451:**591–595.
34. **Tian C, Gao PF, Pinto LH, Lamb RA, Cross TA.** 2003. Initial structural and dynamic characterization of the M2 protein transmembrane and amphipathic helices in lipid bilayers. Protein Sci. **12:**2597–2605.
35. **Grantham ML, Wu WH, Lalime EN, Lorenzo ME, Klein SL, Pekosz A.** 2009. Palmitoylation of the influenza A virus M2 protein is not required for virus replication in vitro but contributes to virus virulence. J. Virol. **83:**8655–8661.
36. **Thaa B, Levental I, Herrmann A, Veit M.** 2011. Intrinsic membrane association of the cytoplasmic tail of influenza virus M2 protein and lateral membrane sorting regulated by cholesterol binding and palmitoylation. Biochem. J. **437:**389–397.
37. **Thaa B, Tielesch C, Möller L, Schmitt AO, Wolff T, Bannert N, Herrmann A, Veit M.** 2012. Growth of influenza A virus is not impeded by simultaneous removal of the cholesterol-binding and acylation sites in the M2 protein. J. Gen. Virol. **93:**282–292.
38. **Hoffmann E, Neumann G, Kawaoka Y, Hobom G, Webster RG.** 2000. A DNA transfection system for generation of influenza A virus from eight plasmids. Proc. Natl. Acad. Sci. U. S. A. **97:**6108–6113.
39. **Zebedee SL, Lamb RA.** 1988. Influenza A virus M_2 protein: monoclonal antibody restriction of virus growth and detection of M_2 in virions. J. Virol. **62:**2762–2772.
40. **Sanan DA, Anderson RG.** 1991. Simultaneous visualization of LDL receptor distribution and clathrin lattices on membranes torn from the upper surface of cultured cells. J. Histochem. Cytochem. **39:**1017–1024.
41. **Ripley BD.** 1979. Tests of "randomness" for spatial point patterns. J. R. Stat. Soc. Series B Stat. Methodol. **41:**368–374.
42. **Baddeley A, Turner R.** 2005. Spatstat: an R package for analyzing spatial point patterns. J. Stat. Softw. **12:**1–42.
43. **Ma C, Soto CS, Ohigashi Y, Taylor A, Bournas V, Glawe B, Udo MK, Degrado WF, Lamb RA, Pinto LH.** 2008. Identification of the pore-lining residues of the BM2 ion channel protein of influenza B virus. J. Biol. Chem. **283:**15921–15931.
44. **Stewart SM, Pekosz A.** 2011. Mutations in the membrane-proximal region of the influenza A virus M2 protein cytoplasmic tail have modest effects on virus replication. J. Virol. **85:**12179–12187.
45. **Ripley BD.** 1977. Modelling spacial patterns. J. R. Stat. Soc. Series B Stat. Methodol. **39:**172–212.
46. **Wilson B, Pfeiffer J, Raymond-Stintz M, Lidke D, Andrews N, Zhang J, Yin W, Steinberg S, Oliver J.** 2007. Exploring membrane domains using native membrane sheets and transmission electron microscopy. Methods Mol Biol. **398:**245–261.
47. **Hughey PG, Roberts PC, Holsinger LJ, Zebedee SL, Lamb RA, Compans RW.** 1995. Effects of antibody to the influenza A virus M_2 protein on M_2 surface expression and virus assembly. Virology **212:**411–421.
48. **McCown MF, Pekosz A.** 2006. Distinct domains of the influenza A virus M2 protein cytoplasmic tail mediate binding to the M1 protein and facilitate infectious virus production. J. Virol. **80:**8178–8189.
49. **Iwatsuki-Horimoto K, Horimoto T, Noda T, Kiso M, Maeda J, Watanabe S, Muramoto Y, Fujii K, Kawaoka Y.** 2006. The cytoplasmic tail of the influenza A virus M2 protein plays a role in viral assembly. J. Virol. **80:**5233–5240.
50. **Drin G, Antonny B.** 2010. Amphipathic helices and membrane curvature. FEBS Lett. **584:**1840–1847.
51. **Shen H, Pirruccello M, De Camilli P.** 2012. SnapShot: membrane curvature sensors and generators. Cell **150:**1300–1300.e2. doi:10.1016/j.cell.2012.08.017.
52. **Jensen MB, Bhatia VK, Jao CC, Rasmussen JE, Pedersen SL, Jensen KJ, Langen R, Stamou D.** 2011. Membrane curvature sensing by amphipathic helices: a single liposome study using α-synuclein and annexin B12. J. Biol. Chem. **286:**42603–42614.
53. **Schmidt NW, Mishra A, Wang J, Degrado WF, Wong GCL.** Influenza virus A M2 protein generates negative Gaussian membrane curvature necessary for budding and scission. J. Am. Chem. Soc., in press.